J Solid State Electrochem (2004) 8: 638–643
DOI 10.1007/s10008-004-0504-2

ORIGINAL PAPER

D. Marrero-López · J. C. Ruiz-Morales · D. Pérez-Coll
P. Núñez · J. C. C. Abrantes · J. R. Frade

Stability and transport properties of $La_2Mo_2O_9$

Received: 11 April 2003 / Accepted: 29 September 2003 / Published online: 23 March 2004

Abstract $La_2Mo_2O_9$ samples were prepared from freeze-dried powder precursors and characterized by XRD, TG/DTA, SEM, electrical and electrochemical measurements. Pellets with different density were obtained by sintering at temperatures between 900 and 1100 °C to obtain nearly dense samples with grain sizes in the range 1–8 μm. The electrical conductivity was measured using impedance spectroscopy. The capacitance and relaxation frequencies of the main contributions to the spectra were used to ascribe the contributions of grain interiors and internal interfaces, and their temperature dependence. A coulometric titration technique was used to evaluate the change of oxygen stoichiometry under moderately reducing conditions, and to estimate the stability limits under strongly reducing conditions. An ion-blocking method was used to evaluate the onset of n-type conductivity, and a combination of these results with total conductivity measurements was used to obtain the ionic transport number. A combination of oxygen stoichiometry changes and ion-blocking results was used to obtain estimates of mobility.

Presented at the OSSEP Workshop "Ionic and Mixed Conductors: Methods and Processes", Aveiro, Portugal, 10–12 April 2003

D. Marrero-López · J. C. Ruiz-Morales · D. Pérez-Coll
P. Núñez (✉)
Departamento de Química Inorgánica,
Universidad de La Laguna,
38200 La Laguna,
Tenerife, Spain
E-mail: pnunez@ull.es
Tel.: +34-922-318501
Fax: +34-922-318461

J. C. C. Abrantes
ESTG, Instituto Politécnico de Viana do Castelo,
4900 Viana do Castelo, Portugal

J. R. Frade
Departamento de Engenharia Cerâmica e do Vidro,
CICECO, Universidade de Aveiro,
3810-193 Aveiro, Portugal

Keywords Coulometric titration · Freeze-dried precursor · Ion blocking · Lanthanum molybdenum oxide · Phase transition

Introduction

Lanthanum molybdenum oxide is a novel fast ion conductor at intermediate temperatures and is thus of interest as a solid electrolyte material for numerous electrochemical applications [1, 2, 3]. The ionic conductivity of $La_2Mo_2O_9$ [4] compares with other oxygen ion conductors possessing fluorite or perovskite structures, and exceeds the ionic conductivity of materials with other structure types (e.g. aurivillius, pyrochlore, apatite, etc.) [5, 6, 7, 8].

The transport properties of fluorite-type materials (e.g. CeO_2) and perovskite materials are strongly dependent on additives with lower valence, in order to enhance the concentration of charge carriers (i.e. oxygen vacancies). This is not needed to ensure high ionic conductivity in $La_2Mo_2O_9$, because the structure of this material includes about 10% of vacant intrinsic oxygen sites [9, 10]. These vacant sites thus allow easy migration of oxygen ions.

One of the main limitations of $La_2Mo_2O_9$ is its phase transition, which causes a sudden drop in conductivity. Steep changes in differential thermal expansion and electrical conductivity versus temperature suggest a first-order phase change with a transition temperature close to 560 °C; the thermodynamics of this phase transition have been evaluated from DSC experiments [11]. Prospective applications of this material thus correspond to temperatures higher than about 600 °C, except possibly for composition changes which might stabilize the high-temperature polymorph at lower temperatures also.

Most of the literature on $La_2Mo_2O_9$ has thus been focused on structural studies. However, one cannot neglect the role of minor electronic contributions, for this might set the limits of the electrolytic domain, especially

under reducing conditions. In this work, the transport properties were evaluated by a combination of total conductivity, obtained from impedance spectra, and an ion blocking Hebb–Wagner technique to evaluate the n-type conductivity. The impedance spectra were also used to separate the contributions of grain interiors and grain boundaries, to assess the relative role of internal interfaces, and their dependence on microstructural features and/or firing schedule.

In addition, one must assess the stability limits to be able to assess the applicability range. The present work thus concentrates on these characteristics, by analysing the onset of different phases, and/or mechanical failure, after exposition to strongly reducing atmospheres. Conditions yielding steep changes of oxygen stoichiometry versus oxygen partial pressure were taken as a limit for the stability range.

Experimental

$La_2Mo_2O_9$ precursors were prepared by a freeze-drying method, as described elsewhere [11]. X-ray diffraction patterns were recorded with a Philips X'Pert diffractometer using Cu K_α radiation and a graphite secondary β monochromator. The cell's parameters were determined using the FULLPROF program [12], assisted by WinPlotr for visualization [13].

Simultaneous thermogravimetric and differential thermal analysis (TG/DTA) was recorded on a Perkin-Elmer model Pyris Diamond TG/DTA. The temperature was varied from room temperature up to 900 °C at 10 °C min^{-1} in a nitrogen atmosphere with a flux of 20 cm^3 min^{-1}.

The precursor powders were uniaxially pressed at 125 MPa, to obtain pellets of diameter 9 mm and thickness 1.5–2 mm. These pellets were sintered at 1100 °C for 5 h (sample S1) and 900 °C for 3 h (sample S2). The values of the relative density, estimated from the geometry and weight of the samples, were approximately 98% and 90% for samples S1 and S2, respectively.

The microstructures of the samples were observed by scanning electron microscopy, both on a well-polished surface and after thermal etching (heating for 10 min at 90% of the sintering temperature). Samples were deposited as a pellet on carbon paper supported on a brass cylinder. A thin gold layer was sputtered onto the surface of the samples to improve the conductivity. Scanning electron microscopy was performed with a JEOL 5600 SEM microscope operating at 10 kV. Figure 1 shows the microstructures of samples sintered at 1100 °C (S1) and 900 °C (S2).

Pt electrodes were painted on sintered disks and fired at 900 °C for 20 min. These samples were characterized by impedance spectroscopy (Solartron 1260 FRA), using four Pt wires. The a.c. frequency was varied between 0.1 Hz and 1 MHz using an excitation voltage of 25 mV for the range 900–600 °C and 200 mV for the range 600–250 °C. Analysis of the impedance spectra was made by equivalent circuits using the Zview program [14].

An ion-blocking Hebb–Wagner technique [15, 16] was used to evaluate the electronic conductivity. A disk-shaped sample is electroded with Pt paste, and the electrodes are fired while pressing Pt wires for the electrical contacts. One side of the sample is then pressed against an impervious alumina disk, with a suitable glass ceramic seal blocking oxygen access; this yields ion-blocking conditions on reaching steady-state conditions under cathodic polarization. The steady-state current is thus purely electronic, and the current–voltage dependence can be used to obtain the electronic conductivity as follows [15, 16]:

$$\sigma_e = \left(\frac{A}{L}\right)\frac{dI}{dV} \quad (1)$$

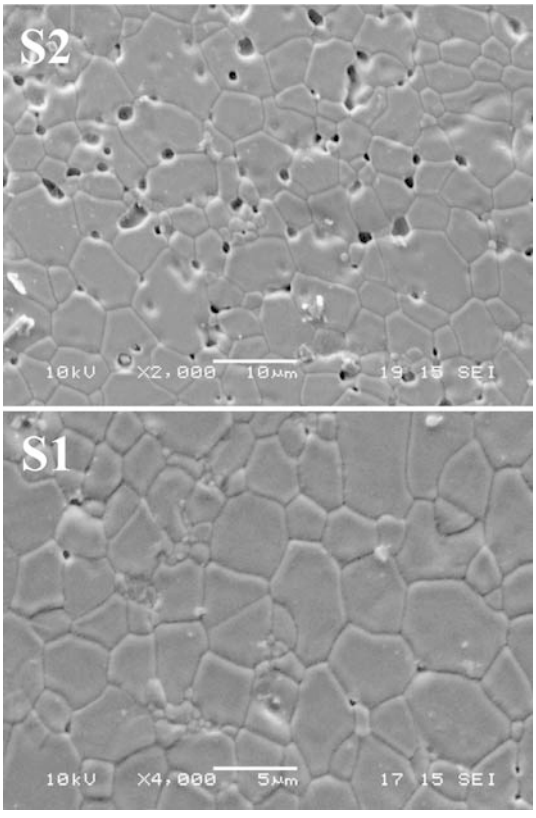

Fig. 1 Scanning electron microstructures of sintered pellets obtained from freeze-dried powder and sintered at 1100 °C for 5 h (S1) and at 900 °C for 3 h (S2)

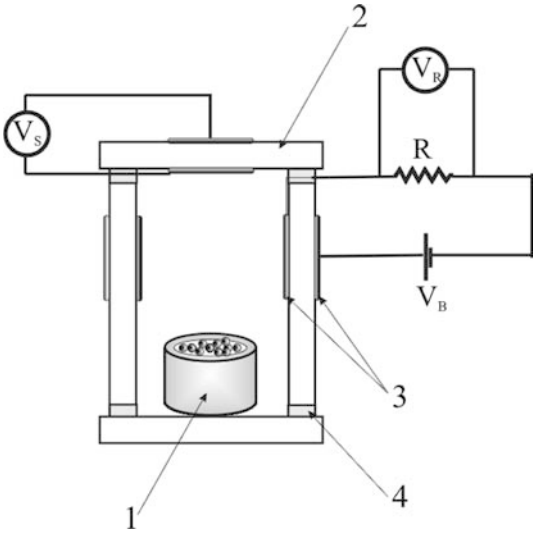

Fig. 2 Schematic representation of the cell used for coulometric titration: (*1*) powder sample being studied; (*2*) YSZ sensor; (*3*) oxygen pump; (*4*) glass sealant; (V_S, V_R) multimeter; (V_B) d.c. source

Coulometric titration measurements were performed using the cell shown schematically in Fig. 2. The cell consists of a section of a YSZ tube with platinum electrodes and used an oxygen pump driven by an external source (Agilent 3646A); this also allows changes in oxygen partial pressure inside the cell by varying the

applied voltage. The cell is closed with two YSZ disks using a glass ceramic sealant. The top YSZ disk was also used as an oxygen sensor to measure the oxygen partial pressure, using a multimeter (Keithley 2700). Powdered $La_2Mo_2O_9$ was placed into a Pt crucible to perform the coulometric titration. A generic step change in oxygen stoichiometry $\Delta\delta$ in the sample ($La_2Mo_2O_{9-\delta}$) was evaluated by taking into account the relevant electrochemical reaction $O^{2-} \rightarrow \frac{1}{2}O_2 + 2e^-$ and integrating the current changes against time, after a step change in the applied voltage:

$$\delta = \frac{M}{2Fm}\int_0^{t'} (I - I_\infty)\mathrm{d}t \quad (2)$$

where M is the molecular weight of $La_2Mo_2O_9$, m is the mass of sample used, F is the Faraday constant, and I_∞ is the residual current due to minor leaks, which might remain nearly uncharged after a very long time t'. The oxygen partial pressure inside the cell was calculated using the Nernst law:

$$Po_2 = P_0 \exp(-4FV_S/RT) \quad (3)$$

where P_0 is the oxygen partial pressure in atmospheric conditions and V_s the read voltage in the YSZ sensor.

Results and discussion

Stability

The limited stability of $La_2Mo_2O_9$ under reducing conditions is demonstrated in Fig. 3; this shows a SEM microstructure of a sample which was exposed overnight to dry 5% H_2/95% Ar. Relatively large cracks are formed, probably due to formation of new phases. These cracks are likely to lead to failure. Further confirmation of this was obtained by X-ray diffraction (Fig. 4). Exposition to dry 5% H_2/95% Ar yields different phases. The phase formed at 900 °C was identified as $La_{2.4}Mo_{1.6}O_8$, with average valence of Mo equal to 5.5, and the phase formed at 800 °C was identified as $La_7Mo_7O_{30}$. Though the original phase α-$La_2Mo_2O_9$ is easily recovered on reverting to oxidizing conditions, the degradation tends to become more severe with additional reduction/oxidation cycles and eventually leads to fracture. The X-ray diffractogram of samples exposed to dry 5% H_2/95% Ar at 700 °C or lower temperatures showed the patterns of α-$La_2Mo_2O_9$.

One can evaluate the stability limits under reducing conditions by taking into account that degradation leads to phases with a lower average valence for Mo, and thus oxygen losses. Coulometric titration results (Fig. 5) were thus used to establish those stability limits. Since the actual changes are somewhat gradual, we assumed that degradation corresponds to an average valence of Mo below 5.5, as found for the new phases detected in the reduced samples. The corresponding oxygen stoichiometry $9-\delta = 8.5$ is reached for typical values of Po_2 in the order of 10^{-13}, 10^{-11} and 10^{-8} Pa at 800, 900 and 1000 °C, respectively.

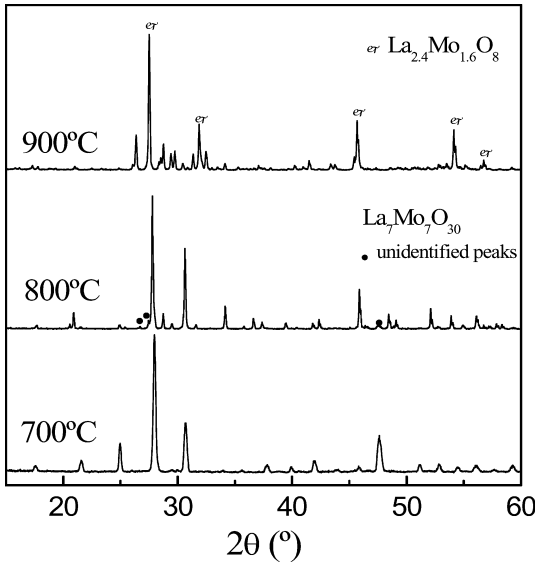

Fig. 4 X-ray diffractograms after exposure to 5% H_2/95% Ar at 900, 800 and 700 °C

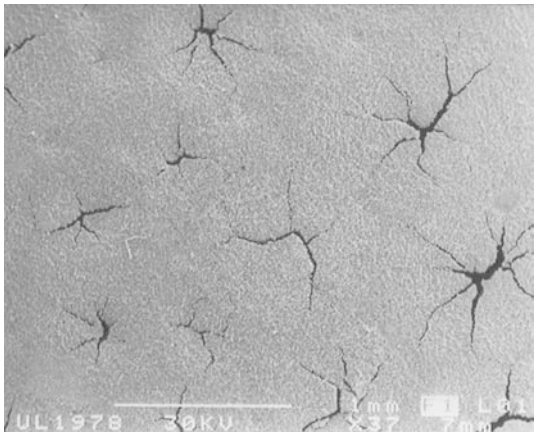

Fig. 3 Cracks on the surface of a sample after exposition to dry 5% H_2/95% Ar at 900 °C

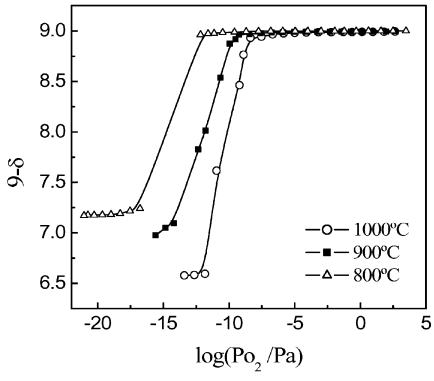

Fig. 5 Massive oxygen stoichiometric changes showing the stability limits at 800, 900 and 1000 °C

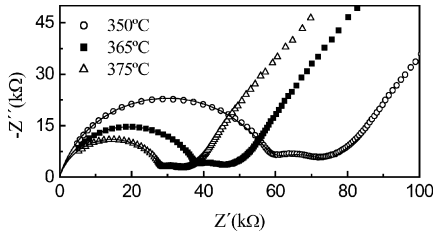

Fig. 6 Impedance spectra of $La_2Mo_2O_9$ pellets sintered at 1100 °C for 5 h (S1). The measuring temperatures are shown on the figure

Electrical conductivity

Typical impedance spectra (Fig. 6) show separate contributions ascribed to the bulk (i.e. grain interiors), in the ranges of high frequency or low capacitance (about 20 pF), and internal interfaces (grain boundaries, pores, segregated inclusions, etc.), in the ranges of intermediate frequency and capacitance (about 27 nF). These contributions correspond to slightly depressed arcs, and an equivalent circuit $(R_BQ_B)(R_{gb}Q_{gb})(R_{el}Q_{el})$ was thus assumed to fit the spectra and to obtain the resistance values of the bulk, R_B, and grain boundaries, R_{gb}, shown in Fig. 7. These results show that higher sintering temperatures yield better microstructures, and thus minimize the internal blocking interfaces.

The total conductivity $\sigma = L/[A(R_B + R_{gb})]$, where L is thickness of the sample and A is the electrode area, also shows the first-order phase transition at about 560 °C, revealed by steep changes in typical Arrhenius representations (Fig. 8):

$$\sigma = \frac{\sigma_0}{T}\exp(-E_a/kT) \tag{4}$$

Values for E_a are shown in Table 1. These results show that the phase transition is reversible on heating and cooling, as demonstrated also by steep changes in the thermal expansion curves and by changes in the unit cell volume [11]. The differences between the results obtained for samples sintered at different temperatures show that poor microstructures still affect the conductivity of the samples at temperatures above the $\alpha \rightarrow \beta$ phase transition.

An ion-blocking method was used to evaluate the electronic conductivity and its dependence on oxygen partial pressure; this yielded the electronic current–voltage dependence shown in Fig. 9, and the corresponding dependence of electronic conductivity on Po_2 (Fig. 10) was extracted from that dependence (Eqs. 1 and 3). These results show the onset of a significant n-type conductivity contribution, especially on approaching the limits of the stability range.

Changes in oxygen stoichiometry (Fig. 11) also indicate the onset of a typical n-type conductivity contribution. On assuming a typical reduction reaction:

$$O_O^x \rightleftharpoons \frac{1}{2}O_2 + V_{\ddot{O}} + 2e^- \tag{5}$$

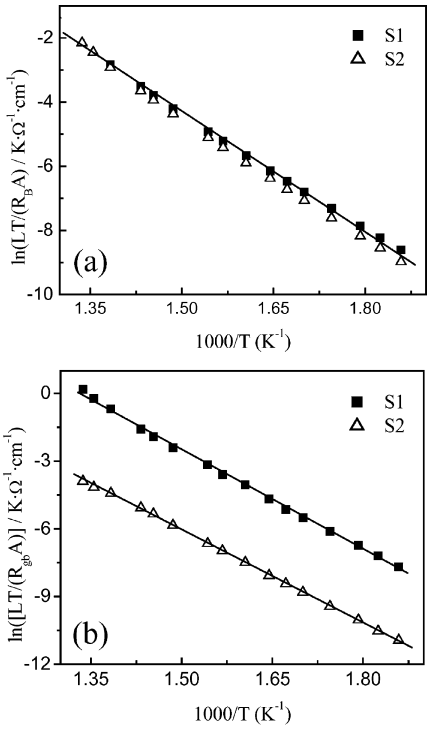

Fig. 7 Arrhenius plot of bulk (**a**) and grain boundary (**b**) results obtained for samples sintered at 1100 °C (S1) and at 900 °C (S2)

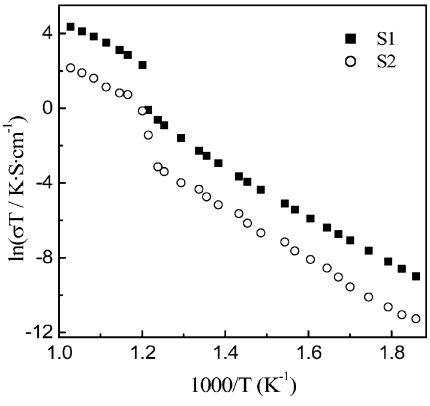

Fig. 8 Total conductivity results showing the differences between samples with poor and good microstructures, and revealing the steep changes at the $\alpha \rightarrow \beta$ phase transition

Table 1 Activation energies of bulk and grain boundary conductivity (gb) of the α-form and activation energies of total conductivity below (LT) and above the phase transition (HT)

Sample	E_a(bulk) (eV)	E_a(gb) (eV)	E_a(LT) (eV)	E_a(HT) (eV)
S1	1.03	1.26	1.11	0.92
S2	1.09	1.17	1.15	0.92

and assuming ideal stoichiometry ($La_2Mo_2O_9$) in air, one can relate the concentration of charge carriers to the measured changes in oxygen stoichiometry (δ in

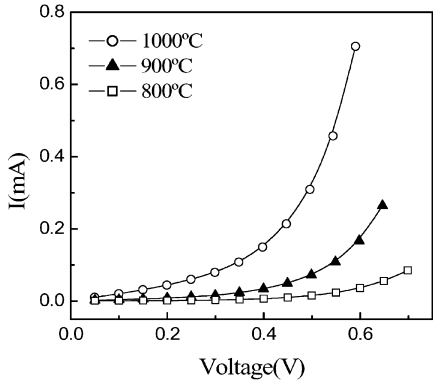

Fig. 9 Ion-blocking results obtained at 800, 900 and 1000 °C

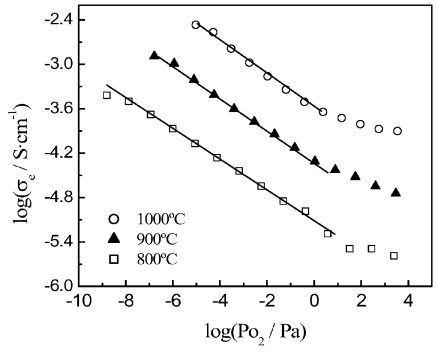

Fig. 10 Electronic conductivity versus oxygen partial pressure, obtained from ion-blocking results

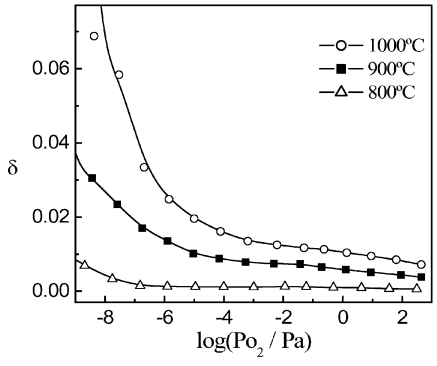

Fig. 11 Oxygen deficiency versus oxygen partial pressure, obtained by coulometric titration

$La_2Mo_2O_{9-\delta}$). These estimates of carrier concentration were thus combined with the electronic conductivity results to obtain the corresponding estimates of mobility, $\mu_e = \sigma_e/(en)$, e being the electronic charge and n the concentration of carriers. The order of magnitude of these estimates (Fig. 12) is close to the mobility of minor electronic species in other ionic conductors.

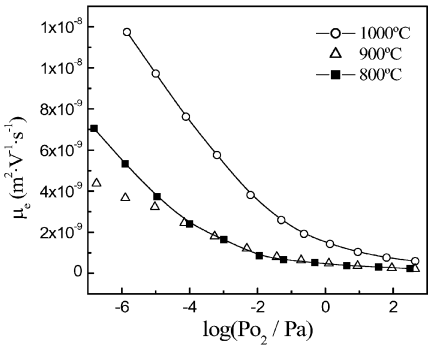

Fig. 12 Estimates of electronic mobility obtained on combining the electronic conductivity and oxygen nonstoichiometry

Conclusions

The conductivity of β-$La_2Mo_2O_9$ is mainly ionic, and compares to the conductivity of ceria-based electrolytes. The ionic transport number remains higher than about 0.98, except possibly for conditions which might lead to degradation under very reducing environments. Though the conductivity of samples with poor microstructures is affected by resistive grain boundaries or other internal interfaces, suitable powder preparation methods and sintering at about 1100 °C yield improved microstructures and conductivity values of about 0.14 S/cm at 800 °C and about 0.03 S/cm at 600 °C. The lower temperature limit for prospective applications is about 560 °C, when the $\beta \rightarrow \alpha$ phase transition causes a sudden drop in conductivity. The applicability of β-$La_2Mo_2O_9$ is also limited to its stability range. Though the stability range reduces to $Po_2 > 10^{-13}$ Pa at 800 °C, this is enhanced at lower temperatures and might still be suitable for SOFC operation.

Acknowledgements The authors acknowledge financial support by the Spanish Research Program MCyT (MAT-2001-3334); by the Canary Islands Government (COFI 2002/027); by FCT, Portugal, under contract POCTI/CTM/39381/2001; and by "Accion Integrada" HP01-82. Also, we wish to thank "Convenio Cajacanarias-ULL" for a grant (D.M.L.) and M.E.C.D. for a F.P.U. grant (D.P.C.).

References

1. Hirschenofer JH, Stauffer DB, Engelman RR, Klett MG (1998) Fuel cell handbook, 4th edn. Publisher, Reading, PA (USA), DOE/FETC-99/1076
2. Minh NQ, Takahashi T (1995) Science and technology of ceramic fuel cells. Elsevier, New York
3. Singhal SC (2000) Solid State Ionics 135:305
4. Lacorre P, Goutenoire F, Bohnke O, Retoux R (2000) Nature 404:856
5. Boivin JC, Mairesse G (1998) Chem Mater 10:2870
6. Kendall KR, Navas C, Thomas JK, Zur Loye HC (1996) Chem Mater 8:642
7. Azad AM, Larose S, Akbar SA (1994) J Mater Sci 29:4135
8. Kudo T (1997) In: Gelling PJ, Bouwmeester HJM (eds) The CRC handbook of solid state electrochemistry. CRC Press, Boca Raton, p 195

9. Goutenoire F, Isnard O, Retoux R, Lacorre P (2000) Chem Mater 12:2575
10. Goutenoire F, Isnard O, Suard E, Bohnke O, Laligant Y, Retoux R, Lacorre P (2001) J Mater Chem 11:119
11. Marrero-Lopez D, Ruiz-Morales JC, Nuñez P, Abrantes JCC (2004) J Solide State Chem (in press)
12. Rodríguez-Carvajal J (2000) FullProf 98. Laboratoire Léon Brillouin, CEA-Saclay, France
13. Roisnel T, Rodríguez-Carvajal J (2003) WinPLOTR, a new tool for powder diffaction. Laboratoire Léon Brillouin, CEA-Saclay, France
14. Zview (2002) A software program for IES analysis. Scribner, Southern Pines, NC, USA
15. Navarro L, Marques F, Frade J (1997) J Electrochem Soc 144:267
16. Lubke S, Wiemhofer HD (1999) Solid State Ionics 17:229